Universiteit Leiden
The Netherlands

Probing quantum puddles: nonlinear dynamics in superfluid film optomechanics

Raabe, L.D.

Citation

Raabe, L. D. (2026, September 8). *Probing quantum puddles: nonlinear dynamics in superfluid film optomechanics*. Retrieved from https://hdl.handle.net/1887/4309261

Version:	Publisher's Version
License:	Licence agreement concerning inclusion of doctoral thesis in the Institutional Repository of the University of Leiden
Downloaded from:	https://hdl.handle.net/1887/4309261

Note: To cite this publication please use the final published version (if applicable).

Chapter 2

Ingredients for superfluid cavity optomechanics experiments

In this chapter, we introduce the reader to the basic ingredients and concepts that we use for our superfluid optomechanics experiment. A brief introduction to a special phase state of Helium at low temperatures called superfluid Helium is given. Optical whispering gallery resonators and evanescent coupling are key aspects of the optical experimental platform that we use to probe thin films of superfluid helium. Furthermore, basic aspects of the field of cavity optomechanics as the interaction mechanism between our optical platform and the mechanics of superfluid helium are introduced. Finally, an overview of the working principles and notable features of our dilution cryostat, that enables ultra-low temperature experiments, is presented.

2.1 Superfluid helium

2.

Helium has one of the simplest electronic structures of any element, but it still displays a range of fascinating and exotic properties. There are two isotopes of helium: helium-4 (^{4}He) and helium-3 (^{3}He), the latter occurring naturally in only about 1 part per million. As a noble gas helium has no permanent electric dipole and the highest ionization energy of any element. The attractive van der Waals force is based on dipole-dipole interactions and weakly acts on helium, due to the zero-point fluctuations of the charge distribution. The zero-point motion of an atom acts against this attractive force and scales inverse to the particle mass and molar Volume, which means it is large for the light helium atom. As atoms are cooled down thermal fluctuations weaken and the attractive van der Waals force is usually stronger than the zero-point fluctuations, leading to the formation of a solid phase with the lowest molar volume. Helium is the only element in which this balance is reversed leading the liquid phase to be energetically favorable over the solid phase (see figure 2.1). Cooling liquid helium-4 below 2.1 Kelvin (at ambient pressure) leads to the formation of a superfluid phase that shows a range of exotic and exciting properties such as flow with zero viscosity [30, 31]. In addition to frictionless flow it shows the fountain effect [32] and the formation of quantized vortices [33]. Most of the observed properties of superfluid helium-4 can be phenomenologically explained by the two-fluid model, that represents the superfluid as an inseparable mixture of superfluid and normal components of helium-4 [34–36]. This model can for example explain the different types of sound propagation in superfluid helium-4, including surface waves on thin films of superfluid helium-4 called third sound [37]. The two fluid model, third sound and its consequences for nonlinear dynamics in thin helium-4 films are discussed in Chapter 3. Helium-3 enters the superfluid phase at temperatures below 1 mK, which makes it challenging to access experimentally. However, it displays even richer superfluid behavior including multiple superfluid phases due to its fermionic nature[9].

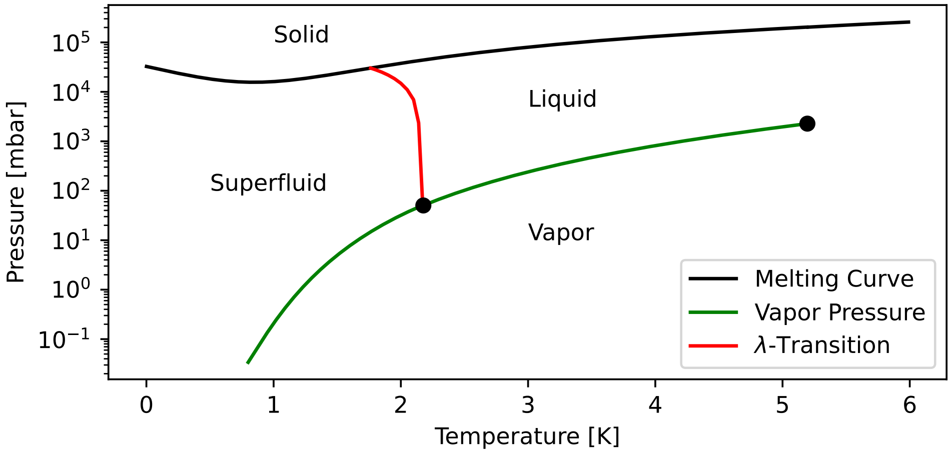

Figure 2.1: Phase diagram for Helium-4. Black points represent the λ Point and the critical point respectively. The phase diagram was drawn using information from [38–41].

2.

2.2 Optical ring resonators

While in traditional optical Fabry-Pérot (FP) cavities light travels back and forth between 2 mirrors, whispering gallery or ring resonators confine light through total internal reflection at the circular periphery of a monolithic structure [42, 43]. In this case, electromagnetic waves are resonant with this structure if a multiple of the wavelength λ matches the circumference of the structure with a radius r

$$m\lambda_{\text{res}} = 2\pi r. \tag{2.1}$$

The associated resonance frequency is $f_{\text{res}} = c/n\lambda_{\text{res}}$, where n is the effective refractive index of the material of the ring resonator. The free spectral range (FSR) of a ring resonator is $FSR = c/2\pi rn$. The internal loss κ_{int} of resonant light circulating in a ring resonator stems from radiative loss due to the curvature, material attenuation and scattering processes. The internal electromagnetic field strength as a function of detuning $\Delta\omega$ from the angular cavity resonance frequency $\omega_{\text{res}} = 2\pi f_{\text{res}}$ follows a Lorentzian distribution:

$$A_{\text{int}}(\Delta\omega) = A_0 \frac{\kappa_{\text{int}}}{\Delta\omega^2 + \kappa_{\text{int}}^2}. \tag{2.2}$$

We can also define an intrinsic quality (Q) factor $Q_0 = 2\omega_{res}/\kappa_{\text{int}}$.

To couple light into an optical resonance of the ring resonator, one should mode-match to the emission pattern of such a lossy structure, which is in general a much more complex waveform than for a FP cavity [43]. Only evanescent field couplers, such as tapered fiber waveguides possess the properties to couple efficiently and robustly to ring resonators. In the presence of a waveguide the optical mode will couple some of the internal power back into the waveguide at a rate κ_{ext} such that the total rate of loss $\kappa = \kappa_{\text{int}} + \kappa_{\text{ext}}$. We can define the coupling efficiency as

$$\eta \equiv \frac{\pi}{\mathcal{F}} \frac{P_{\text{int}}}{P_{\text{ext}}}. \tag{2.3}$$

where we use the Finesse $\mathcal{F} = FSR/\kappa$. The internal electromagnetic field strength in the presence of a waveguide therefore becomes

$$A_{\text{int}}(\Delta\omega) = A_0 \frac{\kappa}{\Delta\omega^2 + \kappa^2}. \tag{2.4}$$

It can be shown that the fraction of transmission through a coupled waveguide on resonance compared to its off-resonance value is given by [43]

$$T = \left(\frac{\tau_{\text{ext}} - \tau_{\text{int}}}{\tau_{\text{ext}} + \tau_{\text{int}}}\right)^2 = 1 - \eta, \tag{2.5}$$

where $\tau_{\text{ext/int}} = 1/\kappa_{\text{ext/int}}$ is the photon lifetime associated with the loss rate (see figure 2.2). In the undercoupling regime, $\kappa_{\text{int}} < \kappa_{\text{ext}}$ and $1 > T > 0$, a fraction of the light from the waveguide is coupled into the ring resonator and the measured effective mode width κ is dominated by the internal loss κ_{int}. At the critical coupling point, $\kappa_{\text{int}} = \kappa_{\text{ext}}$ and $T = 0$. At this point all incoming light is coupled into the ring resonator. In the overcoupling regime $\kappa_{\text{int}} > \kappa_{\text{ext}}$ and $1 > T > 0$ the space between the waveguide and the fiber effectively becomes a lossy cavity supporting spectrally broad optical modes. A significant fraction of the light is coupled into these modes in the overcoupling regime and the effective mode width κ is dominated by the external coupling rate κ_{ext}. While the transmission on resonance of a given optical mode generally does not inform about differences between undercoupling and overcoupling, experimentally one can easily sweep the input frequency over one FSR and record the transmission. At the same coupling efficiency the appearance of additional optical modes with a low Q-Factor in the spectrum indicate the overcoupling regime. This coincides with a drop in the average transmission of the spectrum. For comparatively fewer and narrower modes and a higher average transmission we reside in the

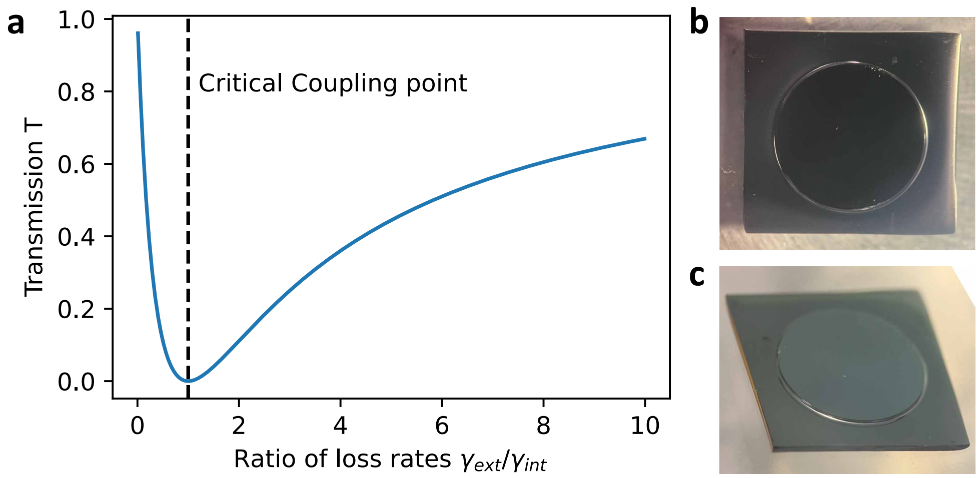

Figure 2.2: Coupling to an optical ring resonator. (a) Transmission on resonance for different loss ratios. The dashed line shows the critical coupling point. To the left is the overcoupling regime and to the right the undercoupling regime. **(b),(c)** Picture of a wedge ring resonator with a radius of 3 mm.

undercoupling regime.

Often the intrinsic Q-factor Q_0 is used to compare different ring resonators, irrespective of their radius. However, in measurements we will always measure the effective mode width, which leads to the so-called loaded Q-factor Q. It is related to the intrinsic Q-factor Q_0 and the coupling Q-factor $Q_c = 4\pi f_{\text{res}}/\kappa_{\text{ext}}$ by

$$\frac{1}{Q} = \frac{1}{Q_0} + \frac{1}{Q_c}. \tag{2.6}$$

For critical coupling it is straightforwad that $Q_0 = Q/2$, but for undercoupling and overcoupling one can show

$$Q_0 = \frac{2Q}{1+\sqrt{T}} \text{ for undercoupling,} \tag{2.7}$$

$$Q_0 = \frac{2Q}{1-\sqrt{T}} \text{ for overcoupling.} \tag{2.8}$$

In general a ring resonator may support many optical modes with slightly different effective round trip lengths. We mainly focus on the fundamental spatial mode[1] (see figure 2.3) as it usually features the highest Q factor Q_0 and provides a larger

[1] The fundamental spatial mode has a Gaussian intensity profile in the transversal direction.

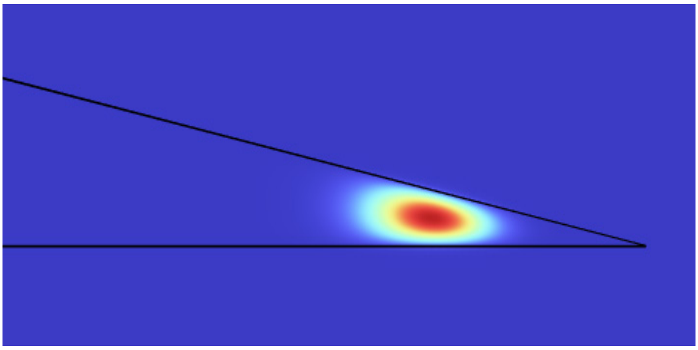

Figure 2.3: Fundamental mode. Graphical representation of the intensity profile of the fundamental mode in the wedge of the optical resonator. Result of a COMSOL simulation.

evanescent field fraction outside of the resonator material.

Optical ring resonators have been made out of many different materials, such as diamond [44], GaAs [45] or Si_3N_4 [46], but one of the most prevalent materials is silica [47] due to its wide transparency region and the advanced microfabrication techniques developed for Silica deposition on Silicon [48]. All devices presented in this thesis are made from silica.

2.3 Cavity optomechanics

Cavity optomechanics studies systems in which at least 1 mechanical degree of freedom couples to an optical cavity [21, 49, 50]. The resonance frequency of an optical cavity changes with the position of the mechanical element. Usually, the mechanical element will have an approximately linear restoring force. The most simple picture of such a system is an optical FP cavity with one mirror suspended on a spring. As the suspended mirror moves, the optical cavity length changes and thus its resonance frequency.

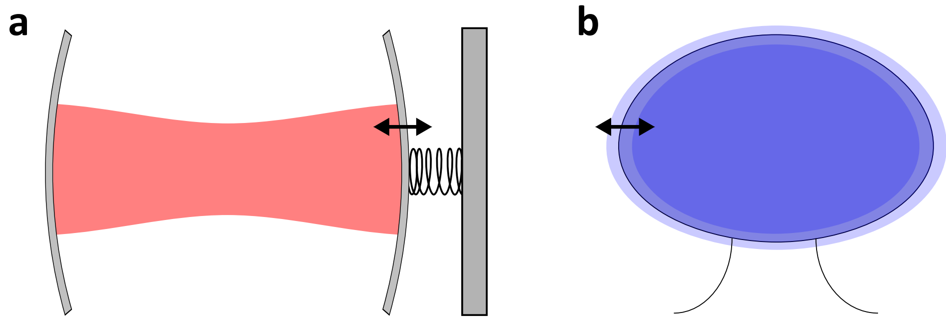

Figure 2.4: Schematic of two optomechanical systems. (a) A free space FP cavity with one mirror suspended by a spring. **(b)** An optical ring-resonator with a thin film of superfluid helium moving radially in and outwards.

This effect can be formalized by introducing the optical angular frequency shift per displacement $G = -\partial\omega/\partial x$. The cavity resonance frequency becomes $\omega_{\text{res}}(x) = \omega_{\text{res},0} - Gx$. We can now find a Hamiltonian for this system by considering the uncoupled mechanical and optical system as harmonic oscillators with angular frequencies Ω_M and ω_{res}:

$$H = \hbar(\omega_{\text{res},0} - Gx)a^\dagger a + \hbar\Omega_M b^\dagger b \tag{2.9}$$

x is the position observable of the mechanical oscillator and can be written as $x = x_0(b + b^\dagger)$, where $x_0 = \sqrt{\frac{\hbar}{2m_{\text{eff}}\Omega_M}}$ is the zero-point fluctuation amplitude of the mechanical oscillator. We have introduced the effective mass m_{eff}, that is in the simplest case just the mass of the mechanical oscillator. However, in more complicated geometries a more complex analysis is needed to find the effective mass. By introducing the single photon optomechanical coupling strength $g_0 = Gx_0$, we can rewrite the optomechanical Hamiltonian as

$$H = \hbar\omega_{\text{res},0}a^\dagger a + \hbar\Omega_M b^\dagger b - \hbar g_0 a^\dagger a(b + b^\dagger). \tag{2.10}$$

The last term is called the interaction Hamiltonian H_{int}. We can find a radiation pressure force acting on the mechanical resonator

$$F_{RP} = -\frac{dH_{\text{int}}}{dx} = \hbar G a^\dagger a. \tag{2.11}$$

The interaction Hamiltonian can be rewritten in the case of an average cavity field $\overline{a} = \sqrt{n_{\text{cav}}}$ and a fluctuation δa. n_{cav} is the average number of intracavity photons.

$$H_{\text{int}} = -(\hbar g_0 |\overline{a}|^2 + \hbar g_0 \sqrt{n_{\text{cav}}}(\delta a^\dagger + \delta a))(b + b^\dagger) + O(|\delta a|^2). \tag{2.12}$$

The first term is an average radiation pressure that can be omitted by shifting the rest position of the mechanical oscillator. The prefactor of the second term is referred to as the optomechanical coupling strength $g = g_0\sqrt{n_{\text{cav}}}$.

2.

While an optical FP cavity with one suspended mirror is the simplest version of an optomechanical system, optomechanical systems with vastly different geometries and effective masses have been studied, ranging from dielectric membranes to single atoms [21]. In this thesis we will discuss an optomechanical system relying on third sound modes in thin superfluid helium films [25].

2.4 Cryostat

For experiments on superfluid Helium, temperatures well below 1 Kelvin (K) are necessary. A reliable way to consistently achieve these temperatures is the use of a ^{3}He-He$_4$ closed-cycle dilution cryostat [51, 52]. The first experimental realization of a dilution refrigerator was achieved in 1964 in the Kamerlingh-Onnes laboratorium at Leiden University [53].

A dilution cryostat generally consists of 4 to 5 plates that are cooled to different temperatures. The plates are called 50 K plate, 4 K plate, Still, (optional 50 mK plate) and mixing chamber (MC) as shown in figure 2.5. Mounting barrels to these plates creates nested radiation shields and vacuum chambers to isolate the innermost parts from the environment. A range of different cooling techniques are then used to achieve extremely low temperatures.

The transition temperature of gas to liquid ^{4}He of 4.2 Kelvin can be reached by adiabatically compressing and expanding ^{4}He gas. A compressor continually compresses ^{4}He gas at room temperature while a pulse tube with a rotating cold head opens and closes a valve, usually at a rate of about 1.5 to 2 Hz. Behind the valve the high pressure Helium gas is allowed to expand, cooling it and the system around it by the use of heat exchangers. The gas is then fed back into the compressor. This process is most efficient at 50 K and is limited to 4.2 K as liquid Helium is no longer compressible. This is the reason to have a 50 K plate that shields radiation from the 4 K plate. One problem arising from this process are unwanted vibrations caused by a mechanical shock each time the Helium gas is allowed to expand. To improve the mechanical stability in our system, the pulse tube has been 'lifted', meaning it is not rigidly bolted to the fridge, but it is instead thermally connected by soft copper ribbons. Additionally, the Still and the plates below are suspended by springs. Eddy-current (EC) dampers are installed between the 4 K plate and the Still to dampen the motion of the suspended plates. Magnets that are rigidly installed to the Still are inserted into grooves cut into a copper block that is rigidly connected to the 4 K plate. If the Still moves with respect to the 4 K plate, the change in magnetic field induces eddy currents in a loop in the copper. The magnetic field created through the current counteracts the magnetic field of the magnets, thus exerting an opposite force on the magnets. The electrical resistance of the copper then dissipates the current as heat, leading to an effective damping of the motion [54]. To further reduce vibrations at the experiment, we suspend it by a mass-spring system acting as two nested mechanical low-pass filters with corner frequencies of $\mathcal{O}(10\ \mathrm{kHz})$ and $\mathcal{O}(10\ \mathrm{Hz})$. The mass spring system can be modeled as an electric circuit with the mass being equivalent to a capacitance and the spring being equivalent to an inductance [55].

To reach temperatures below 4.2 K, ^{4}He gas is condensed in a separate dilution loop and fills a part of the MC, the 50 mK plate and the Still. Pumping on liquid ^{4}He leads to evaporative cooling. The ^{4}He gas that is pumped out is cooled to 4.2 K by the pulse tube loop described above and fed back into the system through the other side of the loop, creating a low and high pressure side of the loop. At a temperature of 1.2 K liquid ^{4}He undergoes a phase transition to superfluid ^{4}He. At this point all ^{4}He atoms are in their motional ground state and vapor pressure becomes extremely low.

We can then introduce ^{3}He gas into the dilution loop. At typical input pressures of 1 to 2 bar ^{3}He gas condenses at temperatures of a few Kelvin. At first, pumping on liquid ^{3}He leads to evaporative cooling as in the case of ^{4}He. However, at a temperature of 870 mK the mixture of ^{3}He and ^{4}He separates into two phases. A highly concentrated ^{3}He phase and a dilute phase containing about 6.6% ^{3}He diluted in ^{4}He. The concentrated phase has a lower density and flows on top of the dilute phase. At the low pressure side of the dilution loop only ^{3}He will evaporate due to its higher vapor pressure leading to a depletion of concentrated ^{3}He phase on this side. Once depleted ^{3}He will start evaporating out of the dilute phase, leading to a drop in the concentration of ^{3}He and a dilution of ^{3}He atoms from the concentrated phase on the

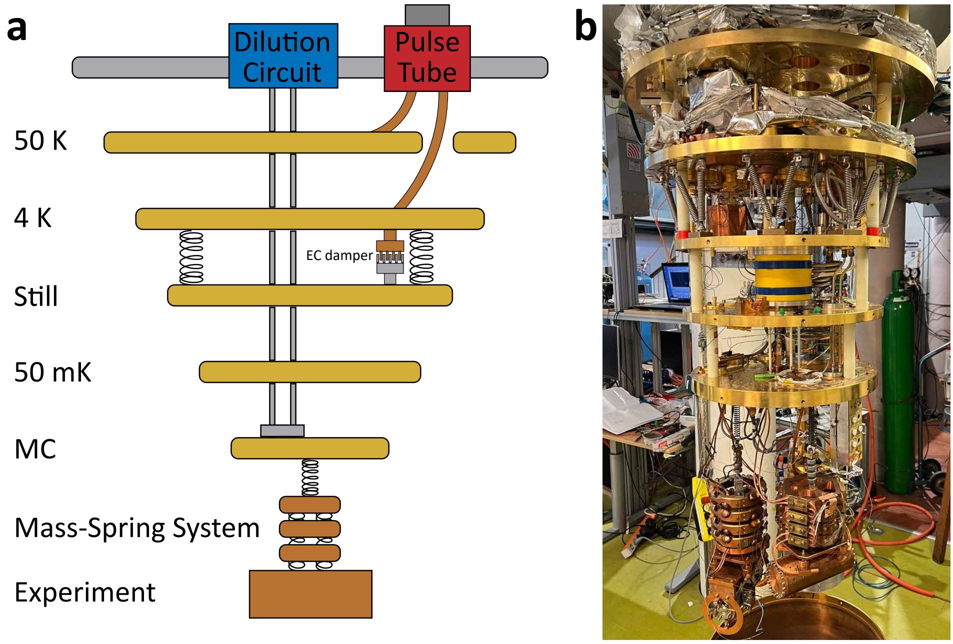

Figure 2.5: Dilution cryostat. (a) Schematic of our dilution cryostat highlighting the different plates and various techniques to reduce vibrations. These include a lifted pulse tube, suspending the still from springs and damping vibrations with an Eddy-current (EC) damper and the use of a mass-spring system. **(b)** Picture of our dilution cryostat with the experimental setup installed at the bottom of a mass-spring system hanging from the MC.

high pressure side into the dilute phase. Dilution of a ^{3}He atom into an ensemble of ^{4}He atoms in the ground state displaces one of the ^{4}He atoms and therefore increases entropy. The increase in entropy in the MC takes energy and therefore leads to cooling. In principle there is no fundamental limit to dilution cooling, but lower temperatures scale unfavorably with the required size of the dilution fridge and cooling power decreases rapidly, leading most dilution fridges to be limited to 10 to 20 mK. Temperatures below 1 mK can be reached by nuclear demagnetization cooling [56].